The Structural Basis for Substrate Specificity and Inhibition of Human *S*-Adenosylmethionine Decarboxylase[†,‡]

W. David Tolbert,[§] Jennifer L. Ekstrom,[§] Irimpan I. Mathews,[§] John A. Secrist III,[||] Preeti Kapoor,[⊥] Anthony E. Pegg,[⊥] and Steven E. Ealick*[,§]

Department of Chemistry and Chemical Biology, Cornell University, Ithaca, New York 14853-1301, Departments of Cellular and Molecular Physiology and of Pharmacology, Milton S. Hershey Medical Center, Pennsylvania State University College of Medicine, Hershey, Pennsylvania 17033, and Southern Research Institute, Birmingham, Alabama 35225-5305

Received April 11, 2001; Revised Manuscript Received June 5, 2001

ABSTRACT: *S*-Adenosylmethionine decarboxylase belongs to a small class of amino acid decarboxylases that use a covalently bound pyruvate as a prosthetic group. It is an essential enzyme for polyamine biosynthesis and provides an important target for the design of anti-parasitic and cancer chemotherapeutic agents. We have determined the structures of *S*-adenosylmethionine decarboxylase complexed with the competitive inhibitors methylglyoxal bis(guanylhydrazone) and 4-amidinoindan-1-one-2′-amidinohydrazone as well as the irreversible inhibitors 5′-deoxy-5′-[*N*-methyl-*N*-[(2-aminooxy)ethyl]amino]adenosine, 5′-deoxy-5′-[*N*-methyl-*N*-(3-hydrazinopropyl)amino]adenosine, and the methyl ester analogue of *S*-adenosylmethionine. These structures elucidate residues important for substrate binding and show how those residues interact with both covalently and noncovalently bound inhibitors. *S*-Adenosylmethionine decarboxylase has a four-layer $\alpha\beta\beta\alpha$ sandwich fold with residues from both β-sheets contributing to substrate and inhibitor binding. The side chains of conserved residues Phe7, Phe223, and Glu247 and the backbone carbonyl of Leu65 play important roles in binding and positioning the ligands. The catalytically important residues Cys82, Ser229, and His243 are positioned near the methionyl group of the substrate. One molecule of putrescine per monomer is observed between the two β-sheets but far away from the active site. The activating effects of putrescine may be due to conformational changes in the enzyme, to electrostatic effects, or both. The adenosyl moiety of the bound ligand is observed in the unusual syn conformation. The five structures reported here provide a framework for interpretation of *S*-adenosylmethionine decarboxylase inhibition data and suggest strategies for the development of more potent and more specific inhibitors of *S*-adenosylmethionine decarboxylase.

S-Adenosylmethionine decarboxylase (AdoMetDC)[1] is essential for the biosynthesis of polyamines and provides a key branch point in the metabolism of *S*-adenosylmethionine (AdoMet) (*1*, *2*). After decarboxylation to form decarboxylated *S*-adenosylmethionine (dcAdoMet), the aminopropyl group of dcAdoMet is transferred either onto putrescine in the synthesis of spermidine or onto spermidine in the synthesis of spermine. Apart from acetylation, which is reversible by an unknown deacetylase, the only metabolic reactions requiring dcAdoMet are those catalyzed by the aminopropyltransferases responsible for the formation of polyamines. AdoMetDC is very tightly regulated in mammalian cells, and the supply of dcAdoMet is linked to the need for polyamine synthesis with only 1−2% of the AdoMet pool being in the form of the decarboxylated derivative (*1*, *3*).

AdoMetDC is one of a small class of decarboxylating enzymes that use a covalently bound pyruvate as a prosthetic group rather than the more generally employed pyridoxal phosphate (*4*, *5*). The generally accepted mechanism for the decarboxylation reaction is depicted in Scheme 1. Both pyruvate and pyridoxal phosphate function by forming a Schiff base with the amino acid substrate, thus facilitating cleavage of the α-carboxylate group and release of carbon

[†] This work was supported by the Biomedical Research Resource Program (RR-01646) and the National Cancer Institute (Grant CA-18138 to A.E.P.) of the National Institutes of Health. S.E.E. is also indebted to the W. M. Keck Foundation and the Lucille P. Markey Charitable Trust

[‡] The coordinates of the AdoMetDC complex structures have been deposited in the Protein Data Bank under the following accession numbers: MeAdoMet, 1I7B; MAOEA, 1I72; MHZPA, 1I79; MGBG, 1I76; CGP48664A, 1I7M.

* To whom correspondence should be addressed at the Department of Chemistry and Chemical Biology, Cornell University, Ithaca, NY 14853. Telephone: (607) 255-7961. Fax: (607) 255-1227. E-mail: see3@cornell.edu.

[§] Cornell University.

[||] Southern Research Institute.

[⊥] Pennsylvania State University College of Medicine.

[1] Abbreviations: AdoMetDC, *S*-adenosylmethionine decarboxylase; HisDC, histidine decarboxylase; AspDC, aspartate decarboxylase; *E. coli*, *Escherichia coli*; AdoMet, *S*-adenosylmethionine; GABA, γ-aminobutyric acid; HPLC, high-performance liquid chromatography; bp, base pair(s); PCR, polymerase chain reaction; TNT, T7-coupled transcription and translation kit; Tris, tris(hydroxymethyl)aminomethane; PEG, poly(ethylene glycol); CCD, charge-coupled device; MGBG, methylglyoxal bis(guanylhydrazone); CGP48664A, 4-amidinoindan-1-one-2′-amidinohydrazone; dcAdoMet, decarboxylated *S*-adenosylmethionine; MeAdoMet, *S*-adenosylmethionine methyl ester; MAOEA, 5′-deoxy-5′-[*N*-methyl-*N*-[(2-aminooxy)ethyl]amino]adenosine; MHZPA, 5′-deoxy-5′-[*N*-methyl-*N*-(3-hydrazinopropyl)amino]adenosine; HEPES, *N*-(2-hydroxyethyl)piperazine-*N*′-2-ethanesulfonic acid; IPTG, isopropylthio-β-D-galactoside; DTT, dithiothreitol.

10.1021/bi010735w CCC: $20.00
Published on Web 07/21/2001

Scheme 1

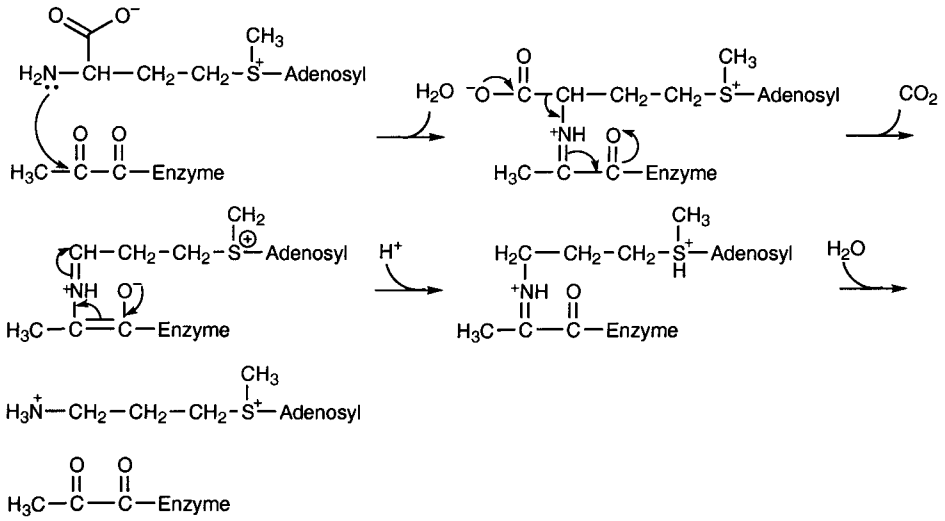

dioxide. Reprotonation of the α-carbon of the product is then necessary to allow Schiff base hydrolysis and release of the product. Although the molecular basis of the mechanism of AdoMetDC is not understood in any detail, studies with site-directed mutagenesis of the totally conserved Cys82 using either the human (*6*) or the *T. cruzi* enzyme (*7*) have implicated this residue as a critical acid/base in the reaction mechanism.

There is good evidence that the enzymes of polyamine biosynthesis in general, and AdoMetDC in particular, may be useful targets for the design of therapeutic agents. Inhibitors of polyamine metabolism have been shown to have potential in chemotherapy and chemoprevention of cancer (*8*−*10*). Furthermore, certain protozoan parasites have been shown to be highly sensitive to compounds interfering with polyamine biosynthesis including AdoMetDC inhibitors (*11*−*14*). This sensitivity may relate to the need for polyamines, a requirement for trypanothione, which is formed from spermidine, and/or to the perturbation of AdoMet and methionine metabolism. AdoMetDC cDNAs have now been cloned and expressed from a variety of parasites that cause serious and widespread human diseases including *Trypanosoma brucei*, *Trypanosoma cruzi* (*15*), and *Plasmodium falciparum* (*16*). An understanding of these enzyme structures and the nature of substrate and inhibitor binding to human and parasite AdoMetDCs would aid in the design of improved inhibitors.

Several approaches to the design of potent and specific inhibitors of AdoMetDC have been taken (*17*). The first approach resulted from the discovery nearly 30 years ago that methylglyoxal bis(guanylhydrazone) (MGBG), which had been shown to have potential as an antineoplastic agent, was a powerful inhibitor of mammalian AdoMetDC (*18*). Many closely related compounds such as the diethyl analogue were also found to be inhibitors of similar or slightly greater potency (*19*), and the strong binding of MGBG to AdoMetDC was exploited for the affinity purification of the enzyme (*20*). Although the underlying reason for the inhibition was unknown, a program of systematic modifications of the MGBG structure was undertaken to attempt to produce more potent inhibitors. In addition, MGBG caused acute toxicity, apparently due to antimitochondrial effects unrelated to its effect on AdoMetDC, and it was hoped that modifications to MGBG might avoid this problem (*9*, *10*). Several compounds with improved properties were obtained (*21*, *22*), including 4-amidinoindan-1-one-2′-amidinohydrazone (CGP48664A) which has been the subject of clinical trials as a cancer therapeutic agent (*23*, *24*).

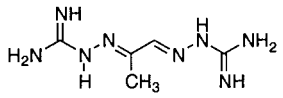

MGBG

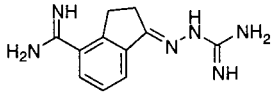

CGP48664A

Mechanism-based approaches to the design of AdoMetDC inhibitors have also led to potential inhibitors. Several compounds have been proposed as enzyme-activated irreversible inhibitors of AdoMetDC, including *S*-(5′-deoxy-5′-adenosyl)-1-ammonio-4-(methylsulfonio)-2-cyclopentene (AdoMac) (*25*) and 5′-{[(*Z*)-4-amino-2-butenyl]methylamino}-5′-deoxyadenosine (AbeAdo) (*26*). AbeAdo was conceived with the idea that the enzyme would act to decarboxylate it and generate a reactive species that would then attack a nucleophilic residue at the active site (*27*). AbeAdo is an excellent inhibitor; however, its inactivation of the human AdoMetDC is through the transamination of the bound pyruvate, which converts to alanine resulting in irreversible inactivation (*28*).

Other compounds that can react irreversibly at the active site by virtue of their ability to form a Schiff base with the pyruvate prosthetic group have been produced (*29*, *30*). These compounds are close analogues of the dcAdoMet reaction product, allowing binding in the correct orientation at the active site but containing a carbonyl-reactive end group in the 5′-side chain. Their mechanism of action has been confirmed by the identification of a peptide from tryptic digests of human AdoMetDC in which the pyruvate is linked in a hydrazone bond to 5′-deoxy-5′-[*N*-methyl-*N*-(3-hydrazinopropyl)amino]adenosine (MHZPA) (*28*).

At present, only one AdoMetDC crystal structure is available, that of the human enzyme (*31*). This structure at 2.25 Å did not contain bound substrate or inhibitor. Although the active site is accurately located by the position of the pyruvate in the structure and those residues that are positioned in the active site cleft can be identified, only a

limited amount of information on the reaction mechanism is provided by this structure. In the present work, we have obtained multiple structures of human AdoMetDC bound to substrate analogues and inhibitors. These include a non-cleavable substrate analogue, MeAdoMet, two covalently linked inhibitors, 5′-deoxy-5′-[*N*-methyl-*N*-[(2-aminooxy)-ethyl]amino]adenosine (MAOEA) and MHZPA, and two reversible inhibitors, MGBG and CGP48664A. These structures show clearly the importance of two phenylalanine residues (Phe7 and Phe223) in the interaction with substrates and inhibitors. Site-directed mutagenesis experiments, which are consistent with this interaction, are also presented. These experiments provide a structural understanding of the AdoMetDC reaction and insight for the development of improved inhibitors.

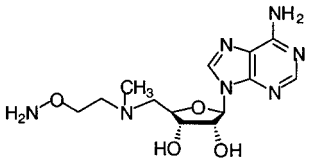

MAOEA

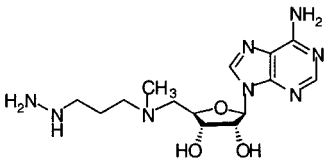

MHZPA

EXPERIMENTAL PROCEDURES

Materials. The T7-coupled transcription and translation (TNT) kit was purchased from Promega (Madison, WI). The Chameleon double-stranded site-directed mutagenesis kit was obtained from Stratagene (La Jolla, CA). The Talon metal affinity resin and Ligation Express kit were products of Clontech (Palo Alto, CA). The pQE30 vector was from Qiagen (Valencia, CA). The restriction enzymes used were from Gibco BRL (Gaithersburg, MD), Promega, and New England BioLabs (Beverly, MA). Sequenase V 2.0 DNA polymerase was from Amersham (Arlington Heights, IL). Human AdoMetDC cDNA was subcloned into the pGEM3Zf$^-$ vector to form pCM9 (*32*) and into the pQE30 vector to form pHIS-SAM (*33*). [^{14}COOH]AdoMet was from Amersham. MGBG was purchased from Aldrich. CGP28864 was a generous gift from Dr. H. Mett, Novartis. MAOEA, MHZPA, and MeAdoMet were synthesized.

Enzyme Expression and Purification. AdoMetDC was purified by the protocol described by Ekstrom et al. (*31*). The human AdoMetDC is in a pQE30 vector adding an N-terminal six-histidine tag and replacing the N-terminal methionine with (MRGS(His)$_6$GS). A small overnight culture of the AdoMetDC expressing JM109 *E. coli* cells was grown in Luria−Bertain (LB) media with 100 μg/mL ampicillin. Larger cultures of LB media and 100 μg/mL ampicillin were then inoculated with a 1:100 dilution (v/v) of the overnight culture. Cells were grown at 37 °C until Abs$_{600}$ reached 0.4, after which 1 mM isopropylthio-β-D-galactoside (IPTG) was added and cells were grown for an additional 4 h. Cells were harvested by centrifugation, resuspended in wash buffer (10 mM imidazole, 20 mM Na_2PO_4, pH 7.4, 500 mM NaCl, 2.5 mM putrescine, and 0.02% Brij-35) with 1 mg/mL lysozyme, and then lysed by sonication or french press. Cellular debris was removed by centrifugation at 20000*g* for 30 min.

The crude cell extract was loaded on a Talon metal affinity resin that had been preequilibrated with wash buffer. The column was washed until the Abs$_{280}$ reached the baseline, typically 5−10 column volumes. The enzyme was eluted with 60 mM imidazole, 20 mM Na_2PO_4, pH 7.4, 500 mM NaCl, 2.5 mM putrescine, and 0.02% Brij-35 and then dialyzed into 10 mM Tris, pH 7.5, 2.5 mM putrescine, 5 mM DTT, 0.1 mM ethylenediaminetetraacetic acid (EDTA), 0.02% Brij-35, and 300 mM NaCl. The enzyme was concentrated, frozen, and stored at −80 °C until used in crystallization experiments.

Purification of the selenomethionine-labeled enzyme was similar to the native enzyme. The cells were first grown in an overnight culture in M9 minimal media supplemented with all the amino acids. Prior to dilution, cells were harvested and washed with M9 minimal media and then resuspended in M9 minimal media supplemented with all the amino acids except methionine, which was replaced with 50 μg/mL selenomethionine. Then 1 mM IPTG was added, and the cells were grown for an additional 24 h. Purification was identical to the native AdoMetDC purification.

Crystallization. All complexes were prepared with wild-type AdoMetDC except for the complex with CGP48664A, in which case selenomethionyl-AdoMetDC was used. Purified enzyme was thawed on ice and then transferred into 200 mM NaCl, 10 mM *N*-(2-hydroxyethyl)piperazine-*N*′-2-ethanesulfonic acid (HEPES), and 1.0 mM dithiothreitol (DTT) with Amicon microcon centrifugal concentrators. Concentrated enzyme (10 mg/mL) was incubated with a 2−5-fold molar excess of MHZPA, MAOEA, or MeAdoMet for 24 h or longer prior to crystallization. The enzyme was used immediately for crystallization in the case of MGBG at 0.2 μM concentration and CGP48664A at a 2 mM concentration. Crystals were grown by the hanging drop method in 10−20% poly(ethylene glycol) (PEG) average molecular weight 8000 (w/w), 100 mM tris(hydroxymethyl)-aminomethane (Tris-HCl), pH 8.0, and 10 mM DTT. Crystallization was carried out at 18 °C except for the CGP48664A complex, which was grown at 4 °C. Crystals grew over a period of a few days, but deteriorated if kept longer than 2−3 weeks.

Data Collection and Processing. Data for the MGBG complex were collected on a Bruker CCD detector with Cu Kα radiation at 18 °C using a capillary-mounted crystal. Data for the CGP48864A, MAOEA, MHZPA, and MeAdoMet complexes were measured using synchrotron radiation and crystals that had been frozen in liquid nitrogen prior to data collection. Crystal quality was strongly dependent on the transfer procedure into the cryoprotectant. Crystals were sequentially transferred into 2, 5, 8, 10, 15, and finally 18% glycerol, 17% PEG 8000 (w/w), 25 mM Tris-HCl, pH 8.0, and 200 mM NaCl with approximately 2 min equilibration time at each step. The MHZPA, CGP48864A, and MeAdoMet complex data sets were measured at CHESS on beam lines A-1 and F-2 using an ADSC Quantum 4 CCD detector. Data for the MAOEA complex were measured at the Advanced Photon Source at Argonne National labs on the COM-CAT beam line using a MAR CCD detector.

The data from CHESS were indexed with the DPS indexing routine (*34*, *35*) and integrated and scaled with MOSFLM and SCALA from the CCP4 suite of processing programs (*36*). Data from the Bruker CCD detector were processed with the accompanying program SAINT. Data from COM-CAT were processed using the DENZO/SCALEPACK data processing programs (*37*). Data collection statistics are summarized in Table 1.

Table 1: Data Collection Statistics for the Five AdoMetDC Complexes

	MAOEA	MHZPA	MeAdoMet	MGBG	CGP48664A
space group	*C2*	*C2*	*C2*	*C2*	$P2_1$
resolution (Å)[a]	2.0(2.07)	2.0(2.15)	1.9(2.01)	2.4(2.49)	2.24(2.39)
cell dimensions	$a = 100.5$ Å	$a = 100.3$ Å	$a = 100.0$ Å	$a = 97.1$ Å	$a = 73.9$ Å
	$b = 50.8$ Å	$b = 50.8$ Å	$b = 51.2$ Å	$b = 45.5$ Å	$b = 55.7$ Å
	$c = 68.9$ Å	$c = 68.6$ Å	$c = 68.5$ Å	$c = 72.1$ Å	$c = 96.1$ Å
	$\beta = 105.3°$	$\beta = 105.3°$	$\beta = 105.4°$	$\beta = 105.2°$	$\beta = 110.4°$
reflections	310436	78987	94520	30563	86417
unique	23342	21309	26560	7718	34984
redundancy	13.2	3.7	3.5	3.9	2.5
completeness(%)[b]	99.2(93.0)	95.7(95.3)	99.6(99.8)	63.7(37.8)	98.4(98.1)
*R*sym(%)[b]	9.2(22.7)	9.8(25.0)	8.1(36.4)	6.5(8.4)	6.7(19.6)
I/σ[b]	16.3(10.3)	5.3(1.4)	7.6(2.2)	8.17(2.0)	4.3(3.2)

[a] The numbers in parentheses represent the low-resolution limits for the high-resolution bins. [b] Numbers in parentheses represent statistics for the highest resolution bins.

Table 2: Refinement Statistics for the Five AdoMetDC Complexes

	MAOEA	MHZPA	MeAdoMet	MGBG	CGP48664A
resolution (Å)	28−2.0	25−2.0	27−1.9	41−2.4	29−2.24
R-factor[a]	0.201	0.212	0.204	0.176	0.242
R-free[a]	0.232	0.256	0.240	0.250	0.294
no. of non-H atoms					
protein	2533	2533	2522	2576	4936
ligand	30	31	34	19	46
water	251	160	185	66	243
B-factors (Å^2)	23.9	23.0	24.7	23.3	19.3
protein (Å^2)	22.9	22.5	24.2	23.1	19.0
ligand (Å^2)	34.2	35.8	27.9	26.8	22.0
putrescine (Å^2)	13.4	15.4	18.1	7.3	3.0
waters (Å^2)	33.7	30.1	31.0	30.1	25.0
rms deviations					
bonds (Å)	0.007	0.006	0.007	0.009	0.019
angles (deg)	1.36	1.32	1.34	1.35	2.28
dihedrals (deg)	25.5	25.5	25.4	25.0	25.

[a] The *R*-factor and *R*-free were calculated relative to F^2 for the synchrotron data and relative to F for the rotating anode data (MGBG).

Structure Determination and Refinement. The structure of the *C2* crystal form of AdoMetDC was determined by molecular replacement using CNS version 1.0 (*38*). Model refinement and automated water addition were also accomplished within CNS (*39*, *40*). Model building was done with the program O (*41*). The ligand molecules were located using composite annealing omit maps based on the appropriate refined AdoMetDC structure. Parameter and topology files were generated from models built into the density and then edited to enforce appropriate structural constraints using modified Engh and Huber (*42*) parameters. A putrescine molecule was clearly visible in the electron densities for all complexes and was added to the models based on the position of putrescine in the 1.5 Å H243A AdoMetDC structure (*43*). Refinement statistics for the five complexes are summarized in Table 2.

Mutagenesis and Plasmid Construction. Point mutations to form mutants F7A and F223A were made in the pCM9 vector using the Chameleon mutagenesis kit following manufacturer's recommendations and using the *Nde*I site for mutant selection. The primers used were 5′-GTCCCTTCG-GCAAAATGTGCAG-3′ for F7A and 5′-CCCACAAG-GATTGGCCATTGTGGCATC-3′ for F223A. The Phe7 mutant cDNA sequence was subcloned into the pQE30 vector using the *Bam*HI and *Sal*I sites. A PCR reaction with the mutant pCM9 as template and primers 5′-GCTAGTCT-CACGGGATCCGAAGCTGC-3′ and 5′-ATTTAGGTGA-CACTATAG-3′ was used to generate a product which was cut with these enzymes and ligated into pQE30. The Phe223 mutant was subcloned into the pQE vector by digesting the mutant pCM9 plasmid with *Bgl*II and *Sal*I and ligating the resulting 1 kb fragment into the 3.5 kb fragment from pHIS-SAM cut with the same enzymes. All of the plasmids were checked by sequencing the entire coding region to ensure that no other mutations were present.

Assay of AdoMetDC Proenzyme Processing and AdoMetDC Activity. To measure the rate of processing of the AdoMetDC proenzyme, the wild-type and mutant AdoMetDC proteins were synthesized in TNT reactions from the pCM9 plasmid, and the rate of formation of the 31 kDa subunit was measured as described earlier (*44*). To measure AdoMetDC activity and response to inhibitors, the his-tagged human wild-type and mutant AdoMetDC proteins were expressed in *E. coli* from the pHIS-SAM plasmid and purified using Talon metal affinity columns as described (*6*). The activity assay measured the ability to convert [^{14}COOH]-AdoMet to $^{14}CO_2$ and dcAdoMet (*44*) in a 15 min assay period. Concentrations of AdoMet ranging from 0.05 to 80 mM were used in a medium containing 50 mM sodium phosphate buffer, pH 6.8, 1.25 mM DTT, and 1 mM putrescine.

Assays were conducted under conditions where less than 10% of the substrate was utilized and there was a linear rate of CO_2 production with time. The substrate concentrations used were varied over the range 0.1−10 times the K_m, and the exact concentrations and specific radioactivity used and

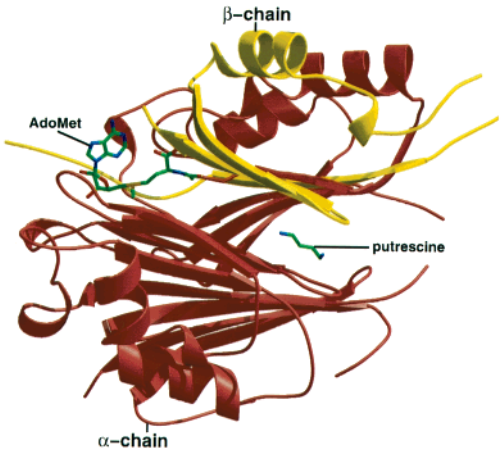

FIGURE 1: *S*-Adenosylmethionine decarboxylase monomer ribbon diagram showing the bound MeAdoMet and putrescine molecules. The β-chain is colored yellow, and the α-chain is colored red. Figures were generated with BOBSCRIPT (*54*, *55*) and RASTER3D (*56*).

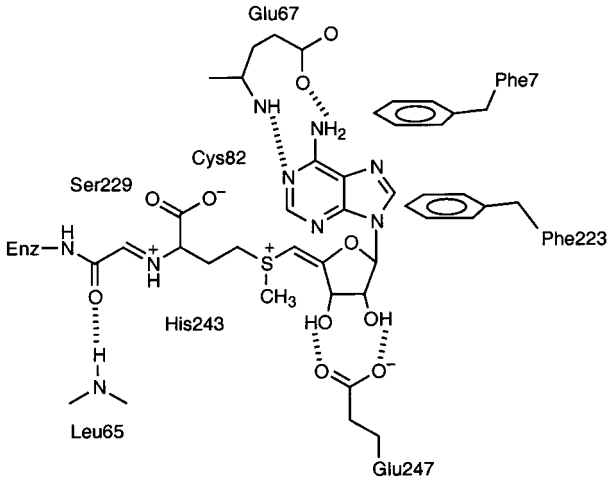

FIGURE 2: Schematic view of the active site of AdoMetDC. The ligand shown is AdoMet based on the structure of MeAdoMet bound to AdoMetDC. Residues that are known to be important for binding or catalysis and that are also near ligands in the three-dimensional structures are shown. Hydrogen bonds are shown as dashed lines. Cys82, Ser229, and His243 are near the substrate, but no specific interactions are observed.

the amount of protein employed varied according to the respective mutants. Sufficient protein was added to ensure that the radioactivity recorded was always more than 4 times the background. Studies of the inhibition of AdoMetDC decarboxylase activity by MGBG and by CGP48664A were carried out by using various concentrations of the inhibitors as previously described (*22*, *23*) at the AdoMet K_m substrate concentration.

RESULTS AND DISCUSSION

Overall Structure of AdoMetDC. AdoMetDC is a $(\alpha\beta)_2$ dimer in which each monomer is a four-layer $\alpha\beta\beta\alpha$ sandwich (Figure 1). Each of the two β-sheets is composed of eight antiparallel β-strands. The initial structure determination revealed that these two sheets have the same topology and that the ($\alpha\beta$) monomer probably arose from a gene duplication event (*31*). The α- and β-subunits (β denoting the smaller subunit by convention) within each monomer are formed by an internal cleavage reaction that also forms the pyruvoyl cofactor. The pyruvoyl group is located in the N-terminal β-sheet (position 68), but both β-sheets participate in substrate binding and catalysis. The active site falls at the edges of the two β-sheets far away from the dimer interface. Putrescine, which activates both the internal cleavage reaction and decarboxylation, is found buried between the two β-sheets, approximately 15−20 Å from the active site.

The tertiary fold of AdoMetDC is different from the other pyruvoyl-dependent amino acid decarboxylases of known structure, *Lactobacillus 30a* histidine decarboxylase (*45*) and *E. coli* aspartate decarboxylase (*46*). AdoMetDC also has a unique fold compared to the entire collection of three-dimensional structures. It differs from other large β-sandwich structures in that there is only one covalent link between the two sheets. Thus, the two β-sheets behave as independently folded domains that can move with respect to each other. In contrast, the lectin family of β-sandwich structures have multiple crossovers between the two sheets creating a more rigid structural unit overall (*47*).

Description of the Active Site of AdoMetDC. The structures of five AdoMetDC complexes define the key active site contacts (Figure 2). As predicted earlier (*31*), the active site is located in a cleft that contains a cluster of highly conserved amino acid residues. The ligands used for the five complexes reported here can be divided into two groups. One group consists of MAOEA, MHZPA, and MeAdoMet, which are substrate analogues. Each contains an adenine base, a ribosyl group, and a 5′-substitutent that is analogous to the 5′-methionyl group of the natural substrate. The other group consists of MGBG and CGP48664A, which are diamidines and competitive inhibitors of AdoMetDC.

The substrate analogues, MAOEA, MHZPA, and MeAdoMet, each form the expected Schiff base with the pyruvoyl group (Figure 3). The pyruvoyl group is in the most buried region of the active site and is highly shielded from the solvent interface. Each of these three ligands contains a four or five-atom linker that joins the ribosyl 5′-position to the pyruvoyl group through a C═N Schiff base linkage. Each linker is in a mostly extended conformation but shows some variation as a result of the chemical differences among the three linker groups. Only MeAdoMet contains a carboxylate group, which is located in a pocket consisting of Phe7, Cys49, Leu65, Glu67, Thr81, Cys82, Thr85, and the adenine base of the substrate, AdoMet. Three residues, Cys82, Ser229, and His243, that are known to be important for either the processing or the decarboxylation reaction (*51*) are located near the 5′-linker. His243 is near the pyruvoyl group, and Ser229 is adjacent to His243 and also near the scissile carboxylate group and the pyruvoyl group. Interestingly, no negatively charged residue is located near the sulfonium group even though biochemical studies demonstrate that ligands that lack this positive charge do not act as substrates or inhibitors (*48*, *49*).

The ribosyl group is located near the active site entrance. The side chain of Glu247, which is absolutely conserved in eukaryotic AdoMetDCs, forms two hydrogen bonds with the ribosyl group. One carboxylate oxygen atom forms a hydrogen bond with the 2′-hydoxyl group, and the other carboxylate oxygen atom forms a hydrogen bond with the 3′-hydoxyl group. The 2′-hydroxyl group is slightly more

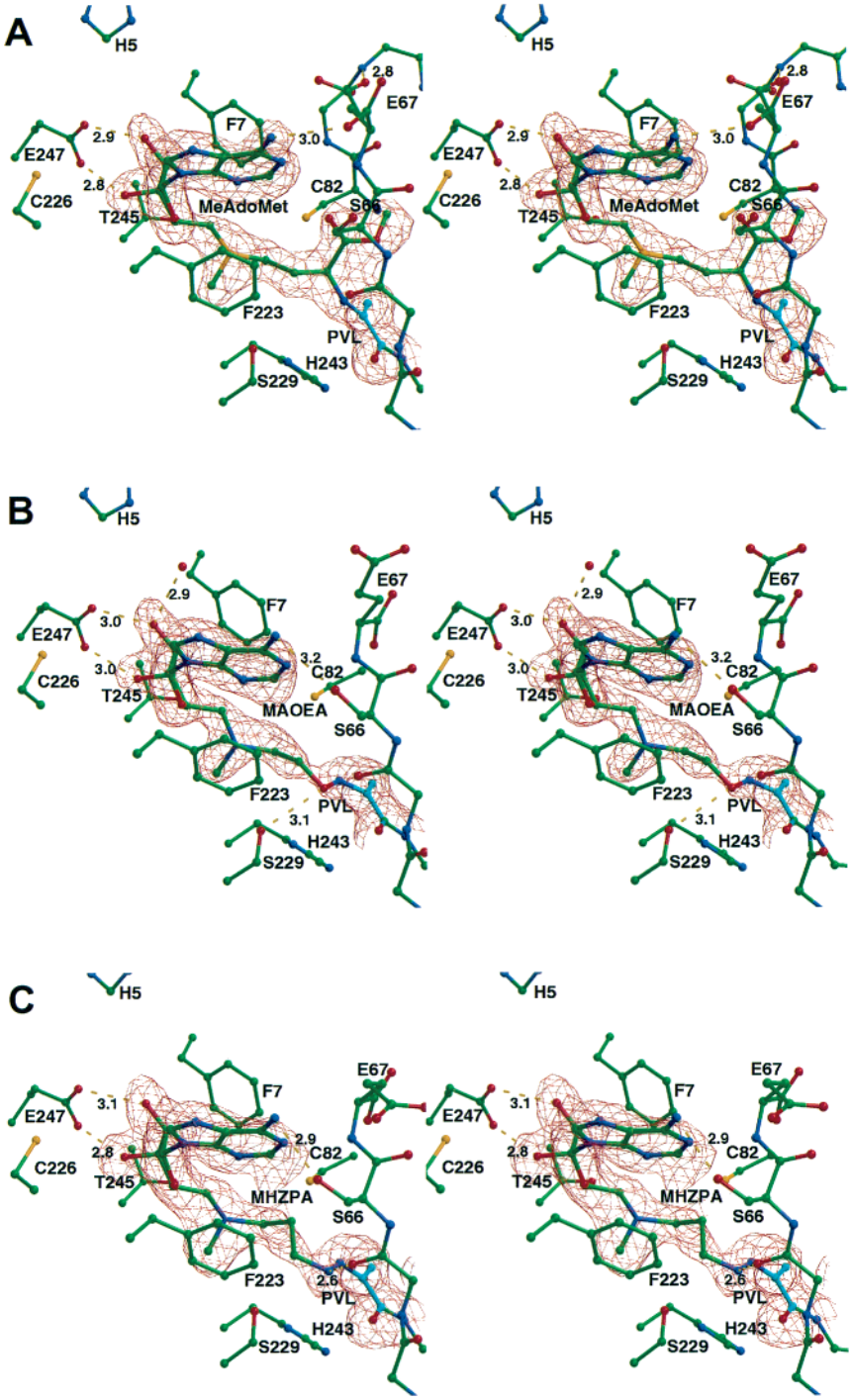

FIGURE 3: Stereoviews of the AdoMetDC complexes. (A) AdoMetDC/MeAdoMet with electron density contoured at 1.0σ. (B) AdoMetDC/MAOEA with electron density contoured at 1.0σ. (C) AdoMetDC/MHPZA with electron density contoured at 0.7σ. For each complex, the side chain atoms in the active site are explicitly drawn. The pyruvoyl group is colored cyan, and backbone atoms for the α-chain N-terminus and the β-chain C-terminus are also explicitly drawn. Hydrogen bonds are shown in yellow, and electron density is in red.

exposed than the 3′-hydroxyl group and in the case of MAOEA hydrogen-bonds to a well-ordered water molecule. The hydrophobic face of the ribosyl group is covered in part by Phe7, which also contacts the adenine base. Thr245 is located nearest the ribose but does not appear to form specific interactions with any ligand atom. Each ribosyl group is bound in the C2′-endo conformation. The positions of the ribose in each of the AdoMet analogue complexes are very similar with coordinates essentially superimposable.

The adenine base joins the ribose in an unusual syn conformation. All three AdoMetDC analogues bind in this conformation with glycosidic torsion angles ranging from 128 to 139°. Binding in the syn conformation places the adenine ring back over the ribosyl group with the adenine N3 atom close to the ribosyl 5′-position. The six-membered ring is positioned toward the deepest part of the active site and further shields the scissile carboxylate group from the active site entrance. The purine five-membered ring points outward toward the solvent with the N7 and C8 positions most exposed. The purine ring is sandwiched between Phe7 and Phe223, which provide stabilizing packing interactions. The adenine has a slightly different tilt in the MAOEA and

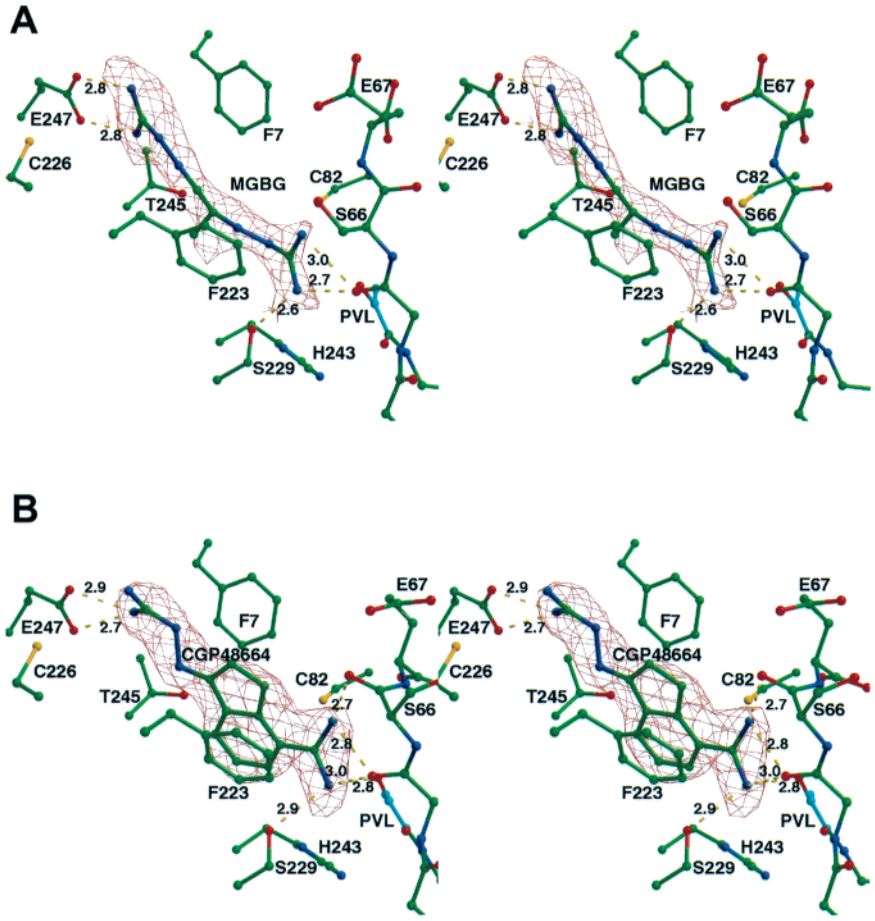

FIGURE 4: Stereoviews of the AdoMetDC complexes. (A) AdoMetDC/MGBG with electron density contoured at 1.0σ. (B) AdoMetDC/CGP48664A with electron density contoured at 1.15σ. Side chain atoms in the active site are explicitly drawn. The pyruvoyl group is in cyan, and backbone atoms for the α-chain N-terminus and the β-chain C-terminus are also explicitly drawn. Hydrogen bonds are shown in yellow, and electron density is in red.

MHZPA complexes relative to the MeAdoMet complex, which is evident in the interactions between the adenine N6 amino groups of the three ligands and the surrounding protein atoms. In the MAOEA and MHZPA complexes, the amino group donates a hydrogen bond to the side chain of Ser66 while in MeAdoMet the amino group donates a hydrogen bond to the terminal carboxylate of the β-chain (residue 67). The difference in hydrogen bonding patterns corresponds to slight differences in the position of the adenine ring relative to Phe223 and Phe7. In addition, in the MeAdoMet complex there is a hydrogen bond between the side chain carboxylate of Glu67 and the main chain nitrogen of Thr84 while in the MAOEA and MHZPA complexes this hydrogen bond does not exist. The conformational difference may be due in part to the presence of the methyl ester, which sits in a pocket near the terminus of the β-chain. The *B*-factors for the adenine base are lower in the MeAdoMet complex than those of the adenine bases in either the MOAEA or the MHZPA complex.

Structures of AdoMetDC/MGBG and AdoMetDC/GCP48664A. The two diamidine inhibitors, MGBG and CGP48664A, bind in a similar manner at the entrance of the AdoMetDC active site (Figure 4). The two inhibitors have similar functional features; however, CGP48664A contains a more rigid bicyclic core. For both complexes, one amidine group interacts through two hydrogen bonds with the highly conserved Glu247. These hydrogen bonds are analogous to the hydrogen bonds formed between the AdoMet ribosyl hydroxyl groups and Glu247. The second amidine group of each diamidine inhibitor forms hydrogen bonds with the side chain of Ser229 and the main chain carbonyl of Leu65. This region is distinctly different from the region occupied by the 6-amino group of AdoMet. In both MGBG and CGP48664A, the linker between the two amidine groups stretches out across the entrance of the active site. The spacers are sandwiched between Phe7 and Phe223, which in the AdoMet analogues provides stabilizing stacking interactions with the adenine ring. For the diamidines, either a longer or a shorter linker would lead to less optimal interactions.

Role of Phe7 and Phe223 in Complex Formation. The structures of AdoMetDC complexes indicate that interactions with the phenyl groups of Phe7 and Phe223 are likely to be important for substrate binding. These residues, which are fully conserved in all known Class 2 AdoMetDCs, were changed individually to alanine by site-directed mutagenesis. These alterations had no significant effect on the processing of the AdoMetDC proenzyme (results not shown). However, the processed enzyme was considerably less active than wild-type AdoMetDC with a 43-fold reduction in the specificity constant (k_{cat}/K_m) for mutant F7A and a 1400-fold reduction for mutant F223A (Table 3). The greatest

Table 3: Kinetic Properties of Human AdoMetDC and Mutants F7A and F223A

protein	k_{cat}/K_m ($s^{-1}M^{-1}$)	k_{cat} (s^{-1})	K_m (mM)	IC_{50} MGBG[a] (μM)	IC_{50} CGP48664A[a] (nM)
wild type	2385	0.31	0.13	0.4	0.23
F7A	55	0.06	1.1	22	250
F223A	1.7	0.02	12.0	62	5000

[a] The kinetics of inhibition of activity were complex and were not strictly competitive. Therefore, results are shown as the amount of inhibitor needed to get 50% inhibition.

effect was on the K_m for AdoMet, which was increased 8.5-fold for F7A and 92-fold for F223A, but the k_{cat} values were also affected, decreasing by 5-fold for F7A and 15-fold for F223A.

The structures of AdoMetDC complexed with MGBG and CGP48664A suggest that these phenylalanine residues represent an important site of interaction with these inhibitors as well. Consistent with this hypothesis, the F7A and F223A mutants were considerably less sensitive to inhibition by MGBG and CGP48664A (Table 3). This effect was particularly marked with CGP48664A, for which there was an 1100-fold decrease in sensitivity for the F7A mutant and a 22 000-fold decrease for the F223A mutant. The values for MGBG increased by 55-fold and 155-fold for F7A and F223A, respectively. This is also consistent with the AdoMet analogue structures in which the adenine base is positioned more closely to Phe223 with a correspondingly larger dipolar interaction between the aromatic rings.

Role of Glu247 in Complex Formation. Glu247 is located near the entrance of the active site and forms strong hydrogen bonds with the hydroxyls of the ribose in the MHZPA, MAOEA, and MeAdoMet complexes and also plays an important role in the binding of MGBG and CGP48664A. In the MHZPA, MAOEA, and MeAdoMet complexes, the ribose assumes a C2′-endo sugar conformation with both hydroxyls forming a bifurcated hydrogen bond with Glu247. In the MGBG and CGP48664A complexes, the guanidyl group of each inhibitor forms a bifurcated hydrogen bond to Glu247 while the imine and amine at the opposite end of each inhibitor form hydrogen bonds to the carbonyl of Leu65 and the pyruvate. The hydrogen bonds or covalent links to the pyruvate on one half of the β-sandwich and the hydrogen bonds to Glu247 on the other half of the β-sandwich for each of the inhibitors emphasize the importance of the relative position of each β-sheet upon inhibitor and substrate binding.

Inhibitor Interactions in the Active Site. The two inhibitors MAOEA and MHZPA have I_{50} values of 400 and 70 nM, respectively, when assayed against the rat AdoMetDC (*50*); the rat AdoMetDC is 97.3% identical in sequence to the human AdoMetDC. Comparing the binding of both in the human AdoMetDC complexes, one can rationalize the difference in affinity between the two. In the MAOEA complex, the oxygen at the position that would correspond to the α-carbon of AdoMet is within hydrogen bonding distance to the hydroxyl of Ser229 (Figure 3A). In the MHZPA complex, one of the nitrogen atoms in the hydrazone is within hydrogen bonding distance to the carbonyl of Leu65 (Figure 3C)—the carbonyl of Leu65 is also important in the binding of MGBG (Figure 4A) and CGP48664A (Figure 4B). The distance between the carbonyl of Leu65 and the amidine group of MGBG/CGP48664A, 2.6 Å, corresponds to a stronger hydrogen bond than is observed in the product analogues. These observations may explain the small but significant difference in the binding of MAOEA and MHZPA.

Catalytic Mechanism of AdoMetDC. The MeAdoMet complex traps the AdoMet analogue as a covalent adduct to the pyruvate and places the ester close to Cys82. The free end of the molecule is fixed by the hydrogen bonds between the ribose hydroxyls and Glu247, the hydrogen bond between the terminal carboxylate group of β-chain residue Glu67 and the adenine nitrogen, and the aromatic interactions between the adenine base and the side chains of Phe7 and Phe223. Elements involved in the binding of the substrate analogue originate from both halves of the β-sandwich within each monomer, with Phe223 and Glu247 on one half of the β-sandwich and Phe7, Glu67, and the pyruvate on the other half. In the complex, Cys82 is located 3.6 Å from the α-carbon of the substrate analogue, making it the closest residue capable of protonating the decarboxyated Schiff base intermediate and regenerating the pyruvate during normal catalysis. These results are therefore in agreement with the suggestion that Cys82 may act as the required proton donor in the human AdoMetDC reaction (*6*). His243, which is 0.9 Å further from the Schiff base intermediate, could potentially serve this role at a lower frequency and may account for the lower rate of turnover, and higher rate of improper protonation and subsequent transamination in the C82A mutant (*6*). $N^{\delta 1}$ of the imidazole ring of His243 is 3.8 Å from the nitrogen of AdoMet and 4.3 Å from the α-carbon of the substrate based on the MeAdoMet complex. The only other side chain in the vicinity is the hydroxyl of Ser229, which is 4.2 Å from the nitrogen and 4.4 Å from the α-carbon of the substrate. It is interesting to note that $N^{\delta 1}$ of the imidazole ring of His243 is within hydrogen bonding distance to the hydroxyl of Ser229 and $N^{\epsilon 2}$ of His243 is within hydrogen bonding distance to the hydroxyls of Ser69 and Thr241. This arrangement may further reduce the occurrence of improper protonation and may also help stabilize the position of the pyruvate, residue 68.

Thr245 is involved in hydrogen bonding to one of two water molecules that are present in the active sites of each AdoMet analogue complex. The two water molecules are within hydrogen bonding distance of each other and are further stabilized by hydrogen bonds to the carbonyl of His243, the carbonyl of Gly9, and the carboxylate of Glu11. The second water molecule is 3.4 Å from Cys82 and may be involved in Cys82-mediated protonation of the Schiff base intermediate. Disruption of the hydrogen bonding network stabilizing these waters may account for the reduction of activity to 11% of wild type in the T245A mutant (*33*).

Schiff Base Formation. A general acid is required for Schiff base formation as well as for the protonation of the intermediate. Again, Cys82 seems to be the most likely candidate residue based on position. Furthermore, a thiol group is consistent with the kinetics of Schiff base formation in the *Trypanosoma cruzi* AdoMetDC (*7*). The mutation of the equivalent cysteine to alanine in the *T. cruzi* AdoMetDC and the inhibition of the enzyme, both human and *T. cruzi* isozymes, with iodoacetic acid support the role of Cys82 in Schiff base formation. As noted above, His243 may take over

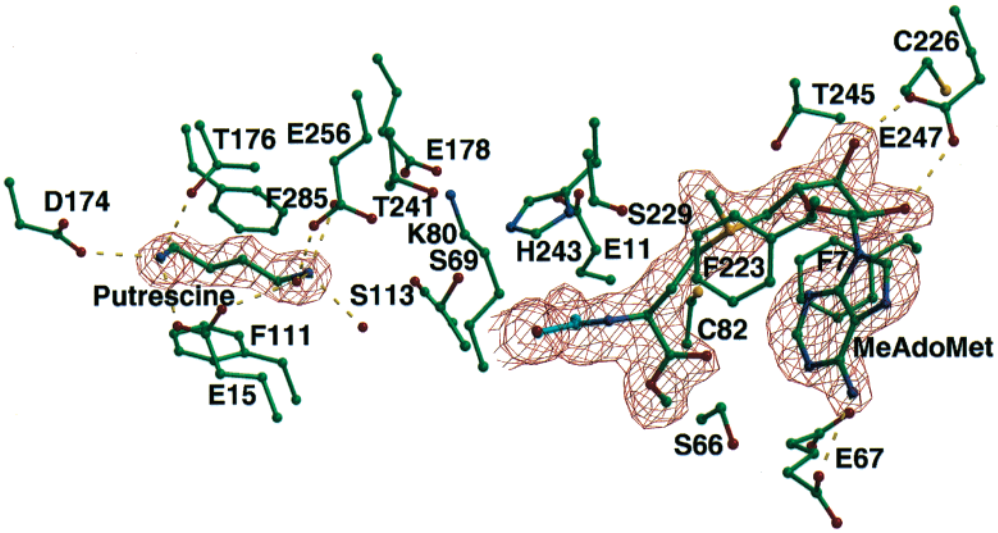

FIGURE 5: AdoMetDC active site and putrescine binding site. Side chain atoms are drawn for key residues that are near either site or that bridge the two sites.

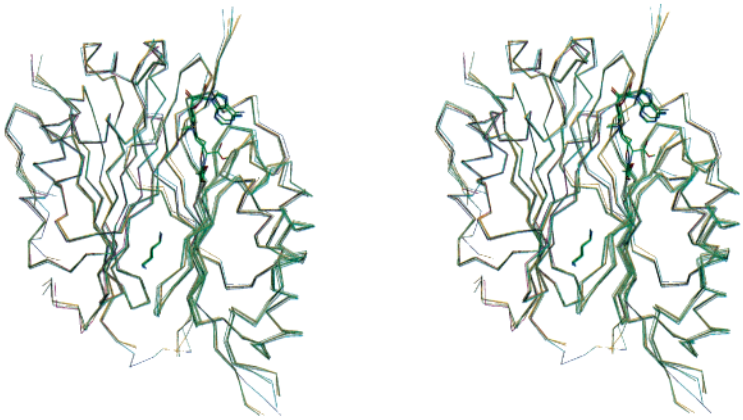

FIGURE 6: Stereoview of a superposition of the AdoMetDC complexes. The α-carbon traces of the MGBG, CGP48664A, MeAdoMet, MAOEA, and MHZPA AdoMetDC complexes were overlaid by the alignment of the left half of the monomer and the resulting positions of the inhibitors shown.

this function in the absence of a cysteine at position 82, but at a lower efficiency.

Effects of Putrescine. The binding of putrescine stimulates AdoMetDC activity mainly due to a lowering of the K_m for the substrate AdoMet (*51*). The putrescine binding site is between the β-sandwich halves, but is 15−20 Å from the decarboxylation site in the MeAdoMet complex (Figure 5). One amino end is stabilized by hydrogen bonds to the carboxylate groups of Glu15 and Asp174, and the hydroxyl of Thr176. The other amino end is stabilized through three bridging waters to the carboxylate groups of Glu15, Glu178, and Glu256 and the hydroxyl of Ser113. The bridging waters have lower than average *B*-factors, less than 20 Å^2, and are well-defined by density. The aliphatic portion of the putrescine packs between the phenyl rings of Phe111 and Phe285. The added stability upon putrescine binding may help in orienting the two halves of the β-sandwich and account for the 4-fold increase in K_m for the substrate in the presence of putrescine.

All five AdoMetDC structures have putrescine bound to the enzyme even though putrescine was not added during crystallization. The recombinant AdoMetDC was produced in *E. coli*, which contains a very high concentration of putrescine (estimated to be about 20 mM) (*52*). Putrescine was also present in the purification buffers at 2.5 mM. It is likely that putrescine is not readily released from the enzyme since the site occupied is relatively buried. These factors probably account for the presence of putrescine in the crystals. Although the structure of the enzyme in the absence of putrescine has not been determined, we speculate based on the extensive hydrogen bonding and charged side chains that putrescine binding causes a shift between the two halves of the β-sandwich.

Evidence for a domain shift comes from a comparison of the structures of AdoMet analogue complexes to the structures of unliganded AdoMetDC and the diamidine inhibitor complexes (Figure 6). In the structures of the substrate and product analogues, the active site opens up slightly, producing approximately a 0.5−0.8 Å shift of one half of the β-sandwich relative to the other when compared to the unliganded AdoMetDC and competitive inhibitor complexes. The overall effect is a slight increase in the distance between the pyruvate and Glu247 to accommodate the substrate. It is possible that the addition of putrescine would cause a similar change in the β-sheet orientation and produce a corresponding change to the active site, thus providing a mechanism for reducing the K_m of the substrate. The abolition of the putrescine activation when any one of the residues

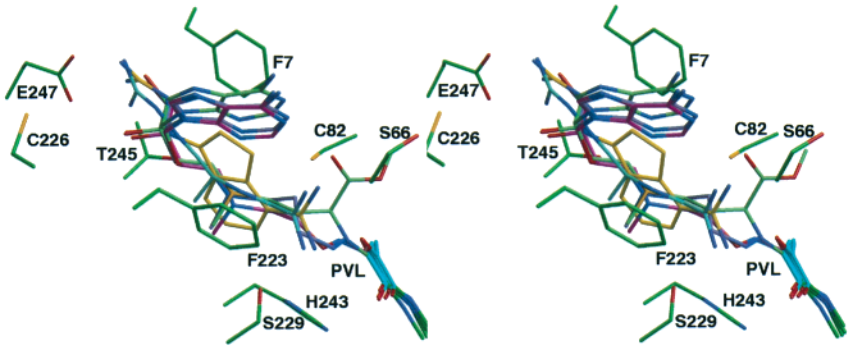

FIGURE 7: Stereoview of the superposition of the five inhibitors. Each inhibitor molecule is drawn in a different color as follows: MGBG, cyan; CGP48664A, magenta; MAOEA, yellow; MHZPA, green; and MeAdoMet, blue.

Glu256, Glu178, or Asp174 is changed to the respective amide (*44*, *53*) is readily explained by this structure since these changes would be expected to interfere with putrescine binding.

An alternate explanation for the stimulatory effects of putrescine is that its binding causes electrostatic effects in the active site. Although the putrescine binding site and active site are separated by about 20 Å, the distance is spanned by a series of conserved charged residues (Figure 5). One end of the putrescine molecule hydrogen-bonds through water molecules to Glu178 and Glu256, which in turn are hydrogen-bonded to Lys80. Lys80, which shows conformational flexibility, is hydrogen-bonded to Glu11, a key catalytic residue.

Implications for Inhibitor Design. A superposition of all five ligands is shown in Figure 7. Although all five ligands generally occupy the same volume in the active site, there are significant differences in the way they interact with surrounding protein atoms. The MeAdoMet complex places the methyl ester in the position in the active site that the carboxylate group would occupy in the substrate prior to decarboxylation. The inhibitors MAOEA and MHZPA, designed with a nitrogen in place of the sulfur in AdoMet and with different functional groups used to form covalent adducts with the pyruvoyl group, demonstrate the flexibility of the link between the pyruvoyl group adduct and the adenosine. They also demonstrate how interactions can influence binding affinities with an additional hydrogen bond between the linker oxygen of MAOEA and the hydroxyl of Ser229 and the second nitrogen of MHZPA's hydrazone and the carbonyl of Leu65. MHZPA has an almost 6-fold lower I_{50} than MAOEA, which may in part be due to the presence of the stronger hydrogen bond in the linker region.

The two product analogues MAOEA and MHZPA and the substrate analogue MeAdoMet also show differences with respect to their interactions with the N6 position of adenine and the hydroxyl group of Ser66 and the terminal carboxylate of Glu67. In addition, the terminal carboxylate and side chain of Glu67 are less well-defined in the MAOEA and MHZPA complexes, indicating an increased flexibility in these product−analogue structures. These differences may reflect structural changes that occur when substrate is converted to product.

The apparent interaction of the substrate with the carboxylate of Glu67 explains the observation that the processed human AdoMetDC generated from the S68C mutant has a greatly reduced activity (*44*). Processing of the S68C mutant generates a pyruvate at the active site but forms a thiocarboxylate group at the terminus of the β-subunit. The noncovalently bound inhibitors MGBG and CGP48664A interact with the carboxylate of Glu247 at one end and with the pyruvate and the carbonyl of Leu65 at the other. In addition to the hydrogen bonds to the functional groups at either end of these molecules, the hydrophobic interactions between Phe7 and Phe223 explain why these compounds are effective inhibitors of AdoMetDC. Because CGP48664A is more rigid than MGBG and because the hydrophobic linker region makes more extensive contacts with the AdoMetDC active site, it is a more potent inhibitor than MGBG. Nevertheless, neither inhibitor fully utilizes the available active site volume or all of the potential active site contacts. Collectively, the five structures of AdoMetDC complexes define the active site for inhibitor design and indicate areas where current inhibitors could be modified to reduce toxicity or increase binding efficiency.

ACKNOWLEDGMENT

Synchrotron X-ray diffraction data for this study were collected at the COM-CAT beam line ID-32 of the Advanced Photon Source and the Cornell High Energy Synchrotron Source. We thank Ms. Leslie Kinsland for her assistance in the preparation of the manuscript.

REFERENCES

1. Pegg, A. E., Xiong, H., Feith, D., and Shantz, L. M. (1998) *Biochem. Soc. Trans. 26*, 580−586.
2. Tabor, C. W., and Tabor, H. (1984) *Adv. Enzymol. Related Areas Mol. Biol. 56*, 251−282.
3. Pegg, A. E., Wechter, R. S., Clark, R. S., Wiest, L., and Erwin, B. G. (1986) *Biochemistry 25*, 379−384.
4. Hackert, M. L., and Pegg, A. E. (1997) in *Comprehensive Biological Catalysis* (Sinnott, M. L., Ed.) pp 201−216, Academic Press, London.
5. van Poelje, P. D., and Snell, E. E. (1990) *Annu. Rev. Biochem. 59*, 29−59.
6. Xiong, H., Stanley, B. A., and Pegg, A. E. (1999) *Biochemistry 38*, 2462−2470.
7. Kinch, L. N., and Phillips, M. A. (2000) *Biochemistry 39*, 3336−3343.
8. Kelloff, G. J., Boone, C. W., Steele, V. E., Lubet, R. A., Doddy, L. A., Malone, W. F., Hawk, E. T., and Sigman, C. C. (1996) *J. Cell. Biochem. Suppl. 26*, 1−28.
9. Marton, L. J., and Pegg, A. E. (1995) *Annu. Rev. Pharmacol. Toxicol. 35*, 55−91.
10. Pegg, A. E. (1988) *Cancer Res. 48*, 759−774.

11. Bacchi, C. J., Nathan, H. C., Yarlett, N., Goldberg, B., McCann, P. P., Bitonti, A. J., and Sjoerdsma, A. (1992) *Antimicrob. Agents Chemother. 36*, 2736−2740.
12. Brun, R., Bühler, Y., Sandmeier, U., Kaminsky, R., Bacchi, C. J., Rattendi, D., Lane, S., Croft, S. L., Snowdon, D., Yardley, V., Caravatti, G., Frei, J., Stanek, J., and Mett, H. (1996) *Antimicrob. Agents Chemother. 40*, 1442−1447.
13. Guo, J., Wu, Y. Q., Rattendi, D., Bacchi, C. J., and Woster, P. M. (1995) *J. Med. Chem. 38*, 1770−1777.
14. Schecter, P. J., Barlow, J. L. R., and Sjoerdsma, A. (1987) in *Inhibition of Polyamine Metabolism. Biological Significance and Basis for New Therapies* (McCann, P. P., Pegg, A. E., and Sjoerdsma, A., Eds.) pp 345−364, Academic Press, Orlando, FL.
15. Persson, K., Aslund, L., Grahn, B., Hanke, J., and Heby, O. (1998) *Biochem. J. 333*, 527−537.
16. Müller, S., Da'dara, A., Lüersen, K., Wrenger, C., Das Gupta, R., Madhubala, R., and Walter, R. D. (2000) *J. Biol. Chem. 275*, 8097−8102.
17. Pegg, A. E., and McCann, P. P. (1992) *Pharmacol. Ther. 56*, 359−377.
18. Williams-Ashman, H. G., and Schenone, A. (1972) *Biochem. Biophys. Res. Commun. 46*, 288−295.
19. Elo, H., Mutikainen, I., Alhonen-Hongisto, L., Laine, R., and Jänne, J. (1988) *Cancer Lett. 41*, 21−30.
20. Pegg, A. E. (1974) *Biochem. J. 141*, 581−583.
21. Regenass, U., Caravatti, G., Mett, H., Stanek, J., Schneider, P., Müller, M., Matter, A., Vertino, P., and Porter, C. W. (1992) *Cancer Res. 52*, 4712−4718.
22. Stanek, J., Caravatti, G., Caprano, H.-G., Furet, P., Mett, H., Schneider, P., and Regenass, U. (1993) *J. Med. Chem. 36*, 46−54.
23. Regenass, U., Mett, H., Stanek, J., Mueller, M., Kramer, D., and Porter, C. W. (1994) *Cancer Res. 54*, 3210−3217.
24. Zhou, H., Choi, L., Lau, H., Bruntsch, U., Vries, E. E., Eckhardt, G., Oosterom, A. T., Verweij, J., Schran, H., Barbet, N., Linnartz, R., and Capdeville, R. (2000) *J. Clin. Pharmacol. 40*, 275−283.
25. Wu, Y., and Woster, P. M. (1992) *J. Med. Chem. 35*, 3196−3201.
26. Danzin, C., Marchal, P., and Casara, P. (1991) in *Enzymes dependent on pyridoxal phosphate and other carbonyl compounds as cofactors* (Fukui, T., Kagamiyama, H., Soda, K., and Wada, H., Eds.) pp 445−447, Pergamon Press, Oxford.
27. Casara, P., Marchal, P., Wagner, J., and Danzin, C. (1989) *J. Am. Chem. Soc. 111*, 9111−9113.
28. Shantz, L. M., Stanley, B. A., Secrist, J. A., and Pegg, A. E. (1992) *Biochemistry 31*, 6848−6855.
29. Artamonova, E. Y., Zavalova, L. L., Khomutov, R. M., and Khomutov, A. R. (1986) *Biorg. Khim. 12*, 206−212.
30. Secrist, J. A., III (1987) *Nucleosides Nucleotides 6*, 73−84.
31. Ekstrom, J. E., Matthews, I. I., Stanley, B. A., Pegg, A. E., and Ealick, S. E. (1999) *Structure 7*, 583−595.
32. Stanley, B. A., Pegg, A. E., and Holm, I. (1989) *J. Biol. Chem. 264*, 21073−21079.
33. Xiong, H., and Pegg, A. E. (1999) *J. Biol. Chem. 274*, 35059−35066.
34. Powell, H. R. (1999) *Acta Crystallogr., Sect. D D55*, 1690−1695.
35. Stellar, I., Bolotovsky, R., and Rossmann, M. G. (1997) *J. Appl. Crystallogr. 30*, 1036−1040.
36. Collaborative Computational Project (Number 4). (1994) *Acta Crystallogr., Sect. D D50*, 760−763.
37. Otwinowski, Z., and Minor, W. (1997) *Methods Enzymol. 276*, 307−326.
38. Brünger, A. T., Adams, P. D., Clore, G. M., DeLano, W. L., Gros, P., Grosse-Kunstleve, R. W., Jiang, J. S., Kuszewski, J., Nilges, M., Pannu, N. S., Read, R. J., Rice, L. M., Simonson, T., and Warren, G. L. (1998) *Acta Crystallogr., Sect. D D54*, 905−921.
39. Kleywegt, G. J., and Brunger, A. T. (1996) *Structure 4*, 897−904.
40. Read, R. (1986) *Acta Crystallogr., Sect. A A42*, 140−149.
41. Jones, T. A., Zou, J.-Y., Cowan, S. W., and Kjeldgaard, M. (1991) *Acta Crystallogr., Sect. A A47*, 110−119.
42. Engh, R. A., and Huber, R. (1991) *Acta Crystallogr., Sect. A A47*, 392−400.
43. Ekstrom, J. L., Tolbert, W. D., Xiong, H., Pegg, A. E., and Ealick, S. E. (2001) *Biochemistry 40*, 9495−9504.
44. Xiong, H., Stanley, B. A., Tekwani, B. L., and Pegg, A. E. (1997) *J. Biol. Chem. 272*, 28342−28348.
45. Gallagher, T., Rozwarski, D. A., Ernst, S. R., and Hackert, M. L. (1993) *J. Mol. Biol. 230*, 516−528.
46. Albert, A., Dhanaraj, V., Genschel, U., Khan, G., Ramjee, M. K., Pulido, R., Sibanda, B. L., von Delft, F., Witty, M., Blundell, T. L., Smith, A. G., and Abell, C. (1998) *Nat. Struct. Biol. 5*, 289−293.
47. Reeke, G., Becker, J., and Edelman, G. (1975) *J. Biol. Chem. 250*, 1525−1547.
48. Pankaskie, M., and Abdel-Monem, M. M. (1980) *J. Med. Chem. 23*, 121−127.
49. Pegg, A. E., and Jacobs, G. (1983) *Biochem. J. 213*, 495−502.
50. Pegg, A. E., Jones, D. B., and Secrist, J. A., III (1988) *Biochemistry 27*, 1408−1415.
51. Stanley, B. A., and Pegg, A. E. (1991) *J. Biol. Chem. 266*, 18502−18506.
52. Tabor, C. W., and Tabor, H. (1985) *Microbiol. Rev. 49*, 81−89.
53. Stanley, B. A., Shantz, L. M., and Pegg, A. E. (1994) *J. Biol. Chem. 269*, 7901−7907.
54. Esnouf, R. (1997) *J. Mol. Graphics 15*, 132−134.
55. Esnouf, R. M. (1999) *Acta Crystallogr., Sect. D D55*, 938−940.
56. Merritt, E. A., and Bacon, D. J. (1997) *Methods Enzymol. 277*, 505−524.

BI010735W